First-principles calculation of thermophysical properties of solids with strong phonon anharmonicity

Terumasa TADANO
Research Center for Magnetic and Spintronic Materials,
National Institute for Materials Science (NIMS),
Sengen, Tsukuba, Ibaraki 305-0047

Abstract

Optimizing thermophysical properties of solids, including thermal expansion, thermal conductivity, and thermodynamic stability is crucial for developing energy- or light-harvesting material that shows a high device performance at operating temperatures. To achieve a simulation-guided design of such materials, lattice vibration (phonon excitation) needs to be modeled accurately beyond the quasi-harmonic level. In recent years, several important theoretical and technical improvements have been made in the field of *ab initio* phonon calculation. These methods have overcome the limitation of the conventional phonon calculation method and further strengthened the predictive power of first-principles calculations based on density functional theory. In this report, we review some of the new computational approaches and demonstrate their validity through applications to a hydrogen-rich superconductor and thermoelectric materials in which phonons are strongly anharmonic.

1 Introduction

Predicting and understanding thermophysical properties of solids only from the crystal structure is crucial for achieving a simulation-guided design of high-performance energy- and light-harvesting materials including but not limited to thermoelectric, photovoltaic, and superconducting materials. For example, lattice thermal conductivity, κ_L, needs to be reduced to achieve a high thermoelectric figure-of-merit ZT. Also, the critical temperature ($T_{\rm c}$) of ferroelectric phase transition plays a crucial role in realizing a giant dielectric constant of polar semiconductors at ambient temperature, as exemplified by the commercially used $BaTiO_3$-based ceramics. Since these finite-temperature thermophysical properties are characterized by the thermal and quantum fluctuation of nuclei, it is necessary to consider the excitation of phonons for achieving a meaningful prediction.

First-principles phonon calculation is performed actively and routinely based on density functional theory (DFT). In most cases, the harmonic approximation (HA) is adapted, assuming that the atomic displacements are much smaller than interatomic distances. While the HA gives reasonable phonon dispersion curves and thermodynamic quantities for many semiconductors and metals, it often becomes inaccurate and sometimes breaks down completely for high-performance thermoelectric and dielectric materials where the atomic displacements can be as large as 10% of an interatomic distance. Moreover, the HA obviously fails to describe physical properties related to the anharmonicity of the potential, including phonon-phonon scattering and structural phase transition. To solve these limitations of the HA, a more advanced phonon calculation method that can include phonon anharmonicity is required.

In the last few decades, several new *ab initio* phonon calculation methods have been proposed as an efficient way to include anharmonic effects [1–7]. Among them, the self-consistent

phonon (SCP) based approaches [3–7] are particularly important because they enable us to access finite-temperature phonon frequencies and polarization vectors as well as T_c values of structural phase transition [8, 9]. Also, the recent advances in thermal transport theory are noteworthy [10, 11]. The advent of these new methods, as well as their efficient implementations in open-source software, have opened up a way to study complicated lattice dynamics in emergent materials and to predict finite-temperature thermophysical properties that cannot be reached by the conventional method.

In this short report, we introduce the basics of the new phonon calculation methods and demonstrate their validity through applications to a hydrogen-rich superconductor, thermoelectric clathrate, and thermoelectric tetrahedrite.

2 Recent progress of *ab initio* phonon calculation

Self-consistent phonon theory

The self-consistent phonon (SCP) theory, which was originally developed by Hooton [12], aims to calculate phonon frequencies and polarization vectors that are renormalized by anharmonicity of the potential. In this theory, an existence of a well-defined *effective* one-body Hamiltonian

$$\mathcal{H}_0 = \sum_{\boldsymbol{q}\nu} \hbar\Omega_{\boldsymbol{q}\nu}\left(b^\dagger_{\boldsymbol{q}\nu} b_{\boldsymbol{q}\nu} + \frac{1}{2}\right) \qquad (1)$$

is assumed. Here, $\boldsymbol{q}$ and ν are the momentum and branch index of phonons, respectively, and $b^\dagger_{\boldsymbol{q}\nu}$ ($b_{\boldsymbol{q}\nu}$) is creation (annihilation) operator of the phonon $\boldsymbol{q}\nu$. The frequency $\Omega_{\boldsymbol{q}\nu}$ is the *effective* frequency that is renormalized by anharmonic effects; therefore, its value differs from the harmonic frequency $\omega_{\boldsymbol{q}\nu}$. In addition, since the *effective* polarization vectors $\{\boldsymbol{\epsilon}_{\boldsymbol{q}\nu}\}$ are also different from the harmonic ones $\{\boldsymbol{e}_{\boldsymbol{q}\nu}\}$, $b^\dagger$ and b in Eq. (1) differ from the creation and annihilation operators of the harmonic Hamiltonian H_0.

Now, let us consider how to determine $\Omega_{\boldsymbol{q}\nu}$ and $\{\boldsymbol{\epsilon}_{\boldsymbol{q}\nu}\}$. To this end, we introduce the exact Hamiltonian H and associated density operator $\rho_H = e^{-\beta H}/\mathrm{Tr}(e^{-\beta H})$, with $\beta = 1/kT$. The Hamiltonian H includes all anharmonic terms; therefore, it may be written as $H = H_0 + U_3 + U_4 + \ldots$ where U_n is the potential energy of the nth-order anharmonicity. By using H and ρ_H, the exact Helmholtz free-energy is given as

$$F_H = \mathrm{Tr}(\rho_H H) + \frac{1}{\beta}\mathrm{Tr}(\rho_H \ln \rho_H). \qquad (2)$$

Next, let us substitute a trial density matrix defined as $\rho_{\mathcal{H}_0} = e^{-\beta\mathcal{H}_0}/\mathrm{Tr}(e^{-\beta\mathcal{H}_0})$ for ρ_H in Eq. (2). We then obtain $F_H(\mathcal{H}_0) = \mathrm{Tr}(\rho_{\mathcal{H}_0} H) + \frac{1}{\beta}\mathrm{Tr}(\rho_{\mathcal{H}_0} \ln \rho_{\mathcal{H}_0})$. By using the Jensen's inequality $e^{\langle X\rangle} \le \langle e^X\rangle$, it is straightforward to show the following Feynman–Gibbs–Bogoliubov inequality holds:

$$F_H \le F_H(\mathcal{H}_0). \qquad (3)$$

In the SCP theory, $\Omega_{\boldsymbol{q}\nu}$ and $\{\boldsymbol{\epsilon}_{\boldsymbol{q}\nu}\}$ are determined so that the right-hand side of Eq. (3) is minimized. This is nothing but a mean-field approximation. Indeed, the SCP theory is a phonon version of the Hartree–Fock theory.

The minimization of $F_H(\mathcal{H}_0)$ can be performed by repeatedly calculating atomic forces in supercells with stochastically sampled atomic configurations and updating the variational parameters in $\mathcal{H}_0$ [5]. An alternative approach we have developed is to derive the SCP equation via the condition of $\partial F_H(\mathcal{H}_0)/\partial X_i = 0$, where X_i comprises all variational parameters including $\Omega_{\boldsymbol{q}\nu}$ and $\{\boldsymbol{\epsilon}_{\boldsymbol{q}\nu}\}$. For the brevity of the explanation, let us assume that the polarization vectors do not change by anharmonic effects. Also, we consider the anharmonic terms up to the fourth-order because fifth- and higher-order terms are less significant. We then obtain the following SCP equation [6, 13]:

$$\Omega^2_{\boldsymbol{q}\nu} = \omega^2_{\boldsymbol{q}\nu} + \frac{1}{2}\sum_{\boldsymbol{q}_1\nu_1} \Phi(\boldsymbol{q}\nu; -\boldsymbol{q}\nu; \boldsymbol{q}_1\nu_1; -\boldsymbol{q}_1\nu_1) \times \frac{\hbar[1 + 2n(\Omega_{\boldsymbol{q}_1\nu_1})]}{2\Omega_{\boldsymbol{q}_1\nu_1}}. \qquad (4)$$

The second term on the right-hand side is the renormalization term associated with the quartic anharmonicity, whose magnitude is proportional to the mean-square displacement of normal coordinate

$\langle Q^*_{\boldsymbol{q}\nu} Q_{\boldsymbol{q}\nu} \rangle = \hbar[1 + 2n(\Omega_{\boldsymbol{q}\nu})]/2\Omega_{\boldsymbol{q}\nu}$ with $n(\omega)$ being the Bose–Einstein distribution function. Since $n(\omega)$ is temperature dependent, the *effective* frequency $\Omega_{\boldsymbol{q}\nu}$ also changes as a function of temperature.

We have shown that Eq. (4) gives phonon dispersion curves of cubic $SrTiO_3$ that agree well with the results of inelastic neutron scattering measurements. Once we compute all quartic coefficients $\Phi(\boldsymbol{q}\nu; -\boldsymbol{q}\nu; \boldsymbol{q}_1\nu_1; -\boldsymbol{q}_1\nu_1)$ in Eq. (4), the *effective* frequencies at various temperatures can be obtained quickly. To compute the quartic coefficients, we first calculate the real-space fourth-order interatomic force constants (IFCs) in a supercell. Then, the real-space IFCs are transformed into the normal coordinate representation $\Phi(\boldsymbol{q}\nu; -\boldsymbol{q}\nu; \boldsymbol{q}_1\nu_1; -\boldsymbol{q}_1\nu_1)$. The computational complexity of this transformation is $\mathcal{O}(N_q^{\text{irred.}} N_{q_1} N_\nu^2)$, where $N_q^{\text{irred.}}$ is the number of irreducible sets of $\boldsymbol{q}$ points, N_{q_1} is the number of $\boldsymbol{q}_1$ points, and N_ν is the number of phonon branches. When we consider the anharmonic mixing of polarization vectors, we also need to compute the off-diagonal elements of the quartic coefficients. In that case, the computational complexity becomes $\mathcal{O}(N_q^{\text{irred.}} N_{q_1} N_\nu^4)$. In our implementation of Eq. (4) in ALAMODE [14], we use a hybrid parallelization of MPI and OpenMP. With this implementation, the SCP calculation has been successfully performed even for complex structures. For example, a SCP calculation of thermoelectric clathrate $Ba_8Ga_{16}Ge_{30}$ ($N_\nu = 162$, $N_q^{\text{irred.}} N_{q_1} = 1$) with the polarization mixing finishes within 10 hours when we use 432 CPU cores of ISSP system B (sekirei).

Phonon scattering

While the SCP method can compute anharmonic phonon frequencies and polarization vectors efficiently, it is still based on a non-interacting picture [Eq. (1)]. Therefore, the phonon linewidth is zero, which leads to the unphysical result that the phonon lifetime and lattice thermal conductivity are infinite. To solve this problem, phonon scattering processes must be considered. In bulk semiconductors, the most dominant source of phonon scatterings is the phonon-phonon scattering associated with the lattice anharmonicity. In the low-temperature region, other scattering processes, including phonon-impurity scattering and phonon-boundary scattering, also become relevant. However, *ab initio* treatment of these extrinsic phonon scatterings is still challenging. Therefore, we will focus on the intrinsic phonons scattering below.

The intrinsic scattering rate of phonons can be obtained by applying many-body perturbation theory to the anharmonic Hamiltonian. Here, the lowest-order perturbation term is the cubic anharmonicity U_3. The unperturbed Hamiltonian may be the true harmonic Hamiltonian H_0, only if all phonons are dynamically stable ($\omega^2_{\boldsymbol{q}\nu} > 0$), or the *effective* one-body Hamiltonian $\mathcal{H}_0$ obtained by an SCP calculation. When we use H_0 as the unperturbed Hamiltonian, the phonon self-energy of the bubble, which gives a first-order correction, is given as [15]

$$\Sigma^{(\mathrm{B})}_{\boldsymbol{q}\nu}(i\omega_m) = \frac{1}{16} \sum_{\boldsymbol{q}_1 \boldsymbol{q}_2} \sum_{\nu_1 \nu_2} \frac{\hbar |\Phi(-\boldsymbol{q}\nu; \boldsymbol{q}_1\nu_1; \boldsymbol{q}_2\nu_2)|^2}{\omega_{\boldsymbol{q}\nu}\omega_1\omega_2} \times \Delta(-\boldsymbol{q} + \boldsymbol{q}_1 + \boldsymbol{q}_2) f(1, 2, i\omega_m), \tag{5}$$

$$f(1, 2, i\omega_m) = \sum_{\sigma=\pm 1} \sigma \left[\frac{1 + n_1 + n_2}{i\omega_m + \sigma(\omega_1 + \omega_2)} - \frac{n_1 - n_2}{i\omega_m + \sigma(\omega_1 - \omega_2)} \right], \tag{6}$$

where $\omega_m = 2\pi m/\beta\hbar$. Here, for the brevity of the notation, we represent $\omega_{\boldsymbol{q}_1\nu_1}$ as ω_1 and $n(\omega_1)$ as n_1. The function $\Delta(\boldsymbol{q})$ in Eq. (5) becomes 1 when $\boldsymbol{q}$ is an integral multiple of the reciprocal lattice vector $\boldsymbol{G}$ and 0 otherwise. Therefore, the double loop over $\boldsymbol{q}$ points in Eq. (5) can be reduced to a single loop. After performing an analytic continuation to the real axis, we obtain the phonon linewidth as $\Gamma^{(\mathrm{B})}_{\boldsymbol{q}\nu} = \mathrm{Im}\Sigma^{(\mathrm{B})}_{\boldsymbol{q}\nu}(\omega_{\boldsymbol{q}\nu})$ and the phonon frequency shift as $\Delta^{(\mathrm{B})}_{\boldsymbol{q}\nu} = -\mathrm{Re}\Sigma^{(\mathrm{B})}_{\boldsymbol{q}\nu}(\omega_{\boldsymbol{q}\nu})$.

In many semiconductors, the linewidth calculated from $\Gamma^{(\mathrm{B})}_{\boldsymbol{q}\nu}$ shows reasonable agreement with experimental data, including its linear temperature-dependence in the high-temperature range. However, in some cases, the theoretical value may un-

derestimate the experimental linewidth most likely due to the presence of additional scattering channels of phonons, including phonon-impurity scattering and higher-order phonon-phonon scatterings. Recently, the self-energies of these additional scattering processes have been evaluated based on DFT for relatively simple systems and reported to be important in correctly understanding the thermal transport behavior [16, 17], which is the main topic of the next subsection.

Thermal transport

First-principles calculation of κ_L has been an active research topic in recent years because its active control would lead to efficient energy conversion and thermal management devices. In particular, significant effort has been placed on elucidating the atomistic-level origin of ultralow thermal conductivity of efficient thermoelectric materials such as intermetallic clathrates and SnSe. To compute κ_L from first principles, the semi-classical Peierls–Boltzmann theory (PBT) is usually adopted. In the PBT, we first assume that the heat flux is carried by phonon quasiparticle; therefore, the heat flux operator is approximated as

$$\boldsymbol{j}_{\rm ph} = \sum_{\boldsymbol{q}\nu} \hbar\omega_{\boldsymbol{q}\nu}\boldsymbol{v}_{\boldsymbol{q}\nu} b^\dagger_{\boldsymbol{q}\nu} b_{\boldsymbol{q}\nu}. \tag{7}$$

Here, $\boldsymbol{v}_{\boldsymbol{q}\nu} = \partial\omega_{\boldsymbol{q}\nu}/\partial\boldsymbol{q}$ is the group velocity of phonon, which is readily obtained from the phonon dispersion curves. Then, after introducing the single-mode relaxation-time approximation, we obtain the thermal conductivity tensor

$$\kappa_{\rm P} = \sum_{\boldsymbol{q}\nu} c_{\boldsymbol{q}\nu}\boldsymbol{v}_{\boldsymbol{q}\nu} \otimes \boldsymbol{v}_{\boldsymbol{q}\nu}\tau_{\boldsymbol{q}\nu}, \tag{8}$$

with $c_{\boldsymbol{q}\nu}$ being the mode specific heat. The phonon lifetime $\tau_{\boldsymbol{q}\nu}$ can be obtained from the phonon linewidth as $\tau_{\boldsymbol{q}\nu} = \hbar/(2\Gamma_{\boldsymbol{q}\nu})$. When we consider the dominant bubble self-energy for $\Gamma_{\boldsymbol{q}\nu}$, the thermal conductivity shows the temperature dependence of $\kappa_L \propto T^{-1}$ in the high-temperature range, in accord with many experimental observation. So far, the PBT-based calculations have been performed for many thermoelectric materials and explained their thermal transport behavior successfully.

While the PBT has been successful for many crystalline solids, it fails to describe the temperature profile of κ_L observed in amorphous solids and other disordered solids. In these systems, the thermal conductivity shows little temperature dependence and does not decrease even in the high-temperature region. To understand thermal transport physics in disordered solids, a beyond PBT treatment would be necessary. One of the most problematic assumptions made within the PBT formalism is the approximation of Eq. (7). More specifically, when we express the harmonic heat flux operator $\boldsymbol{j}^{(2)}$ with the creation and annihilation operators of phonons, we obtain the band diagonal and off-diagonal terms as follows:

$$\begin{aligned}\boldsymbol{j}^{(2)} &= \sum_{\boldsymbol{q}\nu\nu'} \frac{\hbar(\omega_{\boldsymbol{q}\nu}+\omega_{\boldsymbol{q}\nu'})}{2}\boldsymbol{v}_{\boldsymbol{q}\nu\nu'} b^\dagger_{\boldsymbol{q}\nu} b_{\boldsymbol{q}\nu'} \\ &= \boldsymbol{j}_{\rm ph} + \sum_{\boldsymbol{q}\nu\neq\nu'} \frac{\hbar(\omega_{\boldsymbol{q}\nu}+\omega_{\boldsymbol{q}\nu'})}{2}\boldsymbol{v}_{\boldsymbol{q}\nu\nu'} b^\dagger_{\boldsymbol{q}\nu} b_{\boldsymbol{q}\nu'}.\end{aligned} \tag{9}$$

Here, $\boldsymbol{v}_{\boldsymbol{q}\nu\nu'}$ is the band off-diagonal extension of the group velocity. In the PBT, the band off-diagonal terms of the heat flux operator is omitted. In the pioneering work by Allen and Feldman [18, 19], however, they showed that the off-diagonal contribution is dominant in the disordered solids and successfully explained the temperature-dependence of κ_L observed in amorphous silicon. In the Allen–Feldman (AF) theory, however, the effect of phonon scattering is not considered. Therefore, their theory is still not suited for studying thermal transport in disordered solids that also show strong anharmonicity.

Recently, a new thermal transport theory that unifies the PBT and the AF theory has been developed [10]. According to their result, the thermal conductivity is given as

$$\kappa_L = \kappa_{\rm P} + \kappa_{\rm C}, \tag{10}$$

where $\kappa_{\rm P}$ is the Peierls term defined by Eq. (8), and $\kappa_{\rm C}$ is the coherent term associated with the inter-band components of the heat flux operator, which

is given as

$$\kappa_{\mathrm{C}} = \sum_{\boldsymbol{q}} \sum_{\nu \neq \nu'} \frac{c_{\boldsymbol{q}\nu}\omega_{\boldsymbol{q}\nu'} + c_{\boldsymbol{q}\nu'}\omega_{\boldsymbol{q}\nu}}{\omega_{\boldsymbol{q}\nu} + \omega_{\boldsymbol{q}\nu'}} \boldsymbol{v}_{\boldsymbol{q}\nu\nu'} \otimes \boldsymbol{v}_{\boldsymbol{q}\nu'\nu} \times \frac{\Gamma_{\boldsymbol{q}\nu} + \Gamma_{\boldsymbol{q}\nu'}}{(\omega_{\boldsymbol{q}\nu} - \omega_{\boldsymbol{q}\nu'})^2 + (\Gamma_{\boldsymbol{q}\nu} + \Gamma_{\boldsymbol{q}\nu'})^2}. \quad (11)$$

While this new theory has been tested only for a few systems so far, it is expected to improve the prediction accuracy of κ_L and help us deepen our understanding of anomalous thermal transport in strongly anharmonic and/or disordered materials.

Efficient calculation of force constants

So far, we have introduced the state-of-the-art *ab initio* phonon calculation methods. To study phonon-related properties by using these methods, the harmonic, cubic, and quartic IFCs are necessary as inputs. These IFCs can be estimated by repeatedly calculating atomic forces in a supercell with suitably chosen atomic configurations. In the conventional supercell approach, only a few atoms in a supercell are displaced. For instance, the harmonic IFC between atom i and j, Φ_{ij}, is estimated as $\Phi_{ij} = -[F_j(u_i = +h) - F_j(u_i = -h)]/2h$, where $F_j(u_i = \pm h)$ represents the atomic force acting on the atom j when the atom i is displaced slightly ($h \approx 0.01$ Å) from its equilibrium position. This procedure needs to be repeated for all irreducible ij pairs. To estimate the cubic IFC, Φ_{ijk}, in the same fashion, we need to consider, at most, four displacement patterns for each element. Therefore, the number of displacement patterns necessary to obtain all relevant IFCs increases rapidly for the higher-order terms, and the calculation of quartic IFCs would be infeasible or extremely expensive if possible.

To mitigate this issue, we employ the compressive sensing approach [20, 21]. First, to increase the information density obtained from a single DFT calculation, we displace all atoms in a supercell in random directions. For these sampled atomic configurations, we compute the atomic forces; these displacement-force data sets will be served as training data sets of a linear model. Second, instead of calculating the IFC one by one by the central difference, we estimate all IFCs simultaneously by performing linear regression. Since the atomic forces $\boldsymbol{F}$ can be expressed as a linear function of IFCs $\boldsymbol{\Phi}$ as $\boldsymbol{F} = A\boldsymbol{\Phi}$ with A being a sensing matrix comprising atomic displacements, we can estimate the parameter vector $\boldsymbol{\Phi}$ by using ordinary least-squares or other regression methods. In particular, the L_1 penalized regression models such as LASSO are useful because they select and compute physically important IFCs somewhat automatically and set the other irrelevant parameters exactly zero.

We have applied LASSO to various systems and tested its performance. As shown in Fig. 1, the number of static DFT calculations could be reduced dramatically from what would be required if the conventional approach were used. In these LASSO calculations, we gradually increased the training data sets and the cutoff radii of interaction until we obtained an accurate model that reproduces the DFT forces within ∼5% error. The numbers shown for the conventional method are estimated by symmetry argument, where anharmonic IFCs up to the fourth-order are considered within the cutoff radii as the LASSO calculation. The efficient approach, which can be 100 times as efficient as the conventional one, enables us to perform the SCP and PBT calculations of complex systems.

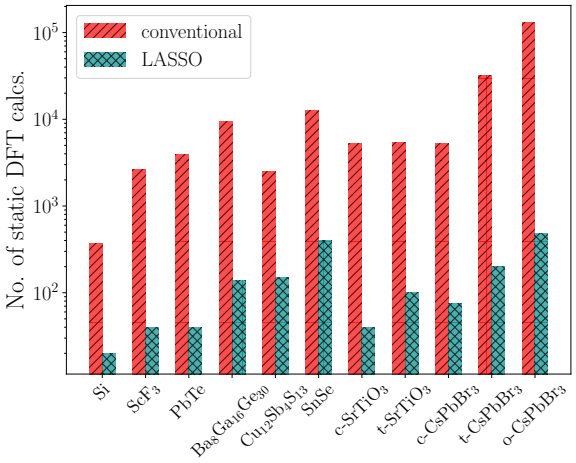

Figure 1: Number of displacement patterns that was used to extract IFCs by LASSO (cyan) compared with the estimated number of patterns required by the conventional approach (red).

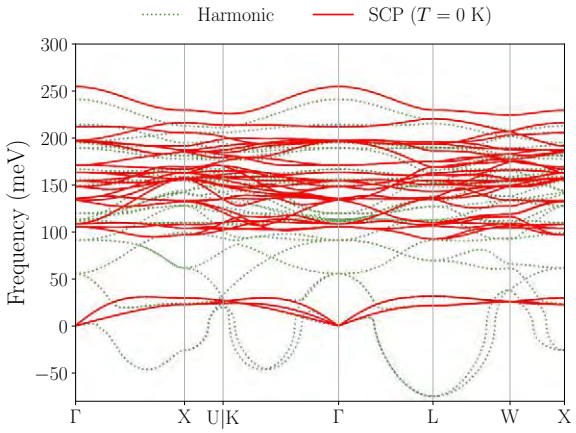

Figure 2: Phonon dispersion curves of $Fm\bar{3}m$-LaH_{10} at 150 GPa calculated within the HA and the SCP theory at $T = 0$ K.

3 Applications

Quantum fluctuation in record superconductor LaH_{10}

Recently, record superconductivity at ∼250 K has been reported for LaH_{10} under the high pressure of 137–218 GPa [22, 23]. The possibility of the high-T_c superconductivity in LaH_{10} was first predicted by DFT calculations [24, 25] and subsequently confirmed experimentally. In the previous DFT predictions, a sodalite-like structure of LaH_{10} with space group $Fm\bar{3}m$ has been suggested as a crystal structure that realizes a high-T_c. However, if the phase stability is evaluated based on enthalpy, LaH_{10} is predicted to be thermodynamically unstable against decomposition below 200 GPa. Moreover, $Fm\bar{3}m$-LaH_{10} is predicted to be dynamically unstable over the whole pressure range where a ∼250 K T_c has been observed experimentally. These contradictions likely indicate the limitation of the conventional computational approaches.

To solve this puzzle, we have performed phonon calculations of LaH_{10} with including anharmonic effects [26]. Figure 2 shows the phonon dispersion of $Fm\bar{3}m$-LaH_{10} calculated within the HA and the SCP theory at 150 GPa. The $Fm\bar{3}m$ structure is dynamically unstable when the HA is employed, indicating the $Fm\bar{3}m$ structure distorts into a low-symmetry structure. Indeed, we have confirmed that the enthalpies of $R\bar{3}m$- and $C2$-LaH_{10} are lower than that of $Fm\bar{3}m$-LaH_{10} by ∼50 meV per formula unit (f.u.) at 150 GPa. However, this conclusion changes when we consider the zero-point motion of hydrogen atoms. As shown in Fig. 2, the quartic anharmonicity renormalizes phonon frequencies significantly and stabilizes the phonons in the entire Brillouin zone even at $T = 0$ K, which is possible due to the large zero-point motion of hydrogen atoms. After obtaining the stable phonons, we have also estimated the zero-point energy (ZPE) and evaluated the relative stability of the $Fm\bar{3}m$ structure over the distorted phases based on enthalpy+ZPE. As a result, the $Fm\bar{3}m$ phase is found to be stable than the $R\bar{3}m$ structure by ∼ 110 meV / f.u., which agrees better with the experimental observation. The inclusion of the ZPE also changes the thermodynamic stability of $Fm\bar{3}m$-LaH_{10}. For example, the formation enthalpy defined as

$$\Delta H[\mathrm{LaH_{10}}] = H[\mathrm{LaH_{10}}] - \frac{7}{8}H[\mathrm{LaH_{11}}] - \frac{1}{8}H[\mathrm{LaH_3}] \quad (12)$$

is about 140 meV/f.u. at 200 GPa, indicating that LaH_{10} decomposes into LaH_3 ($Cmcm$) and LaH_{11} ($P4/nmm$). However, this conclusion changes when we consider the ZPE additionally; the formation enthalpy becomes negative as $\Delta H + \Delta\mathrm{ZPE} = -280$ meV/f.u.

To summarize, our calculations have clearly shown that the large quantum fluctuation of hydrogen nuclei plays a crucial role in stabilizing the highly-symmetric $Fm\bar{3}m$-LaH_{10} over the wide pressure range of 137–218 GPa. We have also calculated the superconducting T_c based on the Migdal–Eliashberg theory and obtained an excellent agreement with the experimental values obtained for LaH_{10} and LaD_{10} [26]. This agreement further confirms that the $Fm\bar{3}m$ phase of LaH_{10} is indeed responsible for the record superconductivity at ∼250 K.

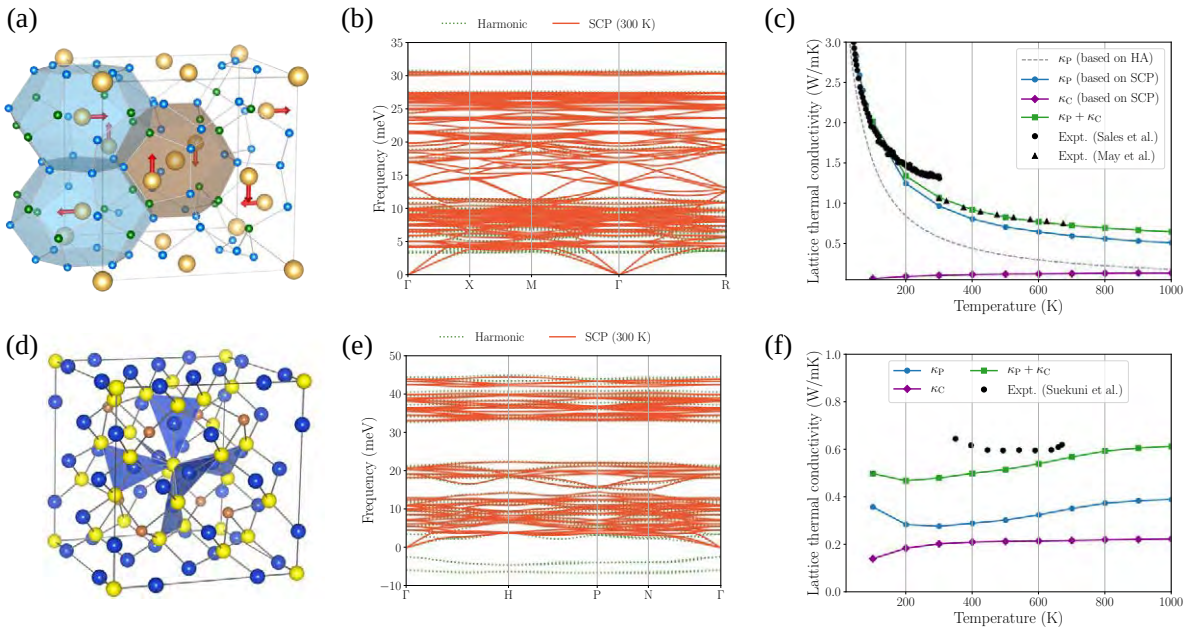

Figure 3: Crystal structures and phonon properties of thermoelectric clathrate $Ba_8Ga_{16}Ge_{30}$ (BGG) and tetrahedrite $Cu_{12}Sb_4S_{13}$. (a) Crystal structures of (a) BGG, adopted from Ref. [27], and (d) tetrahedrite. (b,e) Phonon dispersion curves of BGG and tetrahedrite, respectively, calculated within the HA (dotted lines) and the SCP method at 300 K (solid lines). (c,f) Thermal conductivities of BGG and tetrahedrite, respectively, calculated by different methods. For comparison, the experimental values of Refs. [28–30] are also shown.

Thermal conductivity in complex thermoelectric materials

The thermal transport in complex thermoelectric materials has attracted special attention not only because their thermal conductivity is unusually low but because they sometimes show a *glasslike* temperature dependence even though they possess periodic crystal structures. In this report, we will focus on the origin of the unusual temperature dependence of κ_L observed in type-I clathrate $Ba_8Ga_{16}Ge_{30}$ (BGG) and tetrahedrite $Cu_{12}Sb_4S_{13}$, whose crystal structures are shown in Figs. 3 (a) and (d). In our previous study [31], we have shown that the low-κ_L value of BGG can be attributed to the strong phonon-phonon scattering induced by the presence of low-frequency optical phonons. We could successfully reproduce the experimental κ_L values up to $\sim$ 100 K by using Eq. (8). However, the temperature dependence weaker than $\kappa_L \propto T^{-1}$ could not be explained by the conventional PBT. In $Cu_{12}Sb_4S_{13}$, κ_L is almost temperature independent, which cannot be explained by the conventional PBT. Actually, the HA yields imaginary phonons for $Cu_{12}Sb_4S_{13}$, which hinders a direct application of Eq. (8).

To understand the origin of the unusual temperature dependence in BGG and tetrahedrite, we have recently performed SCP calculations of these complex materials. Also, the thermal conductivity is evaluated based on Eq. (10) for which the SCP eigenvalues and eigenvectors are used as inputs.

Figures 3 (b) and (e) show the calculated phonon dispersion curves of BGG and tetrahedrite, respectively. The phonon dispersion curves calculated within the HA and SCP theory are somewhat similar, particularly for the high-frequency phonon modes. In the low-frequency range, however, we can see notable differences. In BGG, the frequency of low-lying optical phonon modes around 4.5 meV increases with heating. These phonon modes correspond to the collective vibration of Ba guest atoms inside the large cavities made by the host frame-

work, as indicated by the red arrows of Fig. 3 (a). These phonon modes are often called "rattling" motion. In tetrahedrite, the unstable phonon modes exist within the HA. These phonon modes correspond to the collective vibrations of Cu(2) atoms, which are located on the triangle planes made by sulfur atoms (see Fig. 3(d)). Since the displacement of the Cu(2) atoms occur in the direction perpendicular to the triangle planes, these characteristic phonon modes were named "planar rattling" [30]. In our SCP calculations, the planar rattling modes were stabilized by anharmonic renormalization above $\sim$ 80 K.

Next, we have calculated κ_P and κ_C of Eq. (10) separately; the results are compared with available experimental data in Figs. 3 (c) and (f). When we employed the harmonic phonon dispersion in calculating the phonon lifetimes and $\kappa_{\rm P}$, the thermal conductivity was significantly underestimated, as shown by the dashed line of Fig. 3 (c). When the SCP dispersion was used instead, we could reach a nice agreement with the experimental data, including the temperature dependence weaker than $\kappa_L \propto T^{-1}$. Since the low-lying optical phonons strongly hybridize with the heat-carrying acoustic phonons, a little temperature-dependence of the rattling-mode frequency gives rise to the unusual temperature profile of κ_L [27]. The coherent contribution $\kappa_{\rm C}$ calculated from Eq. (11) accounts for about 10% of total κ_L of BGG at 300 K. For tetrahedrite, the temperature dependence of κ_L is more exceptional as shown in Fig. 3 (f). Interestingly, the little temperature dependence can be explained qualitatively by the Peierls term based on the temperature-dependent SCP wave functions. Still, the calculated $\kappa_{\rm P}$ value significantly underestimates the experimental thermal conductivity for the entire temperature range. This discrepancy can be cured by including the coherent term $\kappa_{\rm C}$; the sum of two contributions, $\kappa_{\rm P} + \kappa_{\rm C}$, reproduces the experimental values even quantitatively. Such a large coherent contribution has already been reported for orthorhombic halide perovskite $CsPbBr_3$ [10], where the particle-like thermal transport is hindered by the strong phonon-phonon interaction. We believe the coherent term $\kappa_{\rm C}$ should be significant not only in disordered solids but also in strongly anharmonic (ordered) solids where the phonon linewidths become broad, and the phonon spectral weights overlap with each other.

4 Summary

In this short report, we reviewed the recent development of new phonon calculation methods that can treat the intrinsic effects of lattice anharmonicity beyond the quasiharmonic level. We showed that the self-consistent phonon scheme solves the limitations of the harmonic phonon theory by incorporating the quartic anharmonicity at the mean-field level. Also, the unified theory of thermal transport, which can account for the coherent thermal transport in addition to the particle-like contribution, was shown to better explain the anomalous thermal transport observed in complex thermoelectric materials.

All of the methods focused in this report are already available in the ALAMODE software [32]. We kindly invite interested readers to visit the homepage and try the software.

This work was partially supported by Grant-in-Aid for Scientific Research (number 16H06345) from the Ministry of Education, Culture, Sports, Science and Technology, Japan. A part of the computation in this work was performed using the facilities of the Supercomputer Center, Institute for Solid State Physics, The University of Tokyo. This report is based on the recent studies done in collaboration with K. Suekuni, S. Tsuneyuki, J. A. Flores-Livas, I. Errea, R. Arita, and T. Koretsune.

References

[1] O. Hellman and I. A. Abrikosov: Phys. Rev. B **88** (2013) 144301.

[2] T. Sun, D.-B. Zhang, and R. M. Wentzcovitch: Phys. Rev. B **89** (2014) 094109.

[3] P. Souvatzis, O. Eriksson, M. I. Katsnelson, and S. P. Rudin: Comp. Mater. Sci. **44** (2009) 888.

[4] B. Monserrat, N. D. Drummond, and R. J. Needs: Phys. Rev. B **87** (2013) 144302.

[5] I. Errea, M. Calandra, and F. Mauri: Phys. Rev. B **89** (2014) 064302.

[6] T. Tadano and S. Tsuneyuki: Phys. Rev. B **92** (2015) 054301.

[7] A. van Roekeghem, J. Carrete, and N. Mingo: Phys. Rev. B **94** (2016) 020303.

[8] R. Bianco, I. Errea, L. Paulatto, M. Calandra, and F. Mauri: Physical Review B **96** (2017) 014111.

[9] T. Tadano and S. Tsuneyuki: Journal of the Ceramic Society of Japan **127** (2019) 404 .

[10] M. Simoncelli, N. Marzari, and F. Mauri: Nature Physics **15** (2019) 809.

[11] L. Isaeva, G. Barbalinardo, D. Donadio, and S. Baroni: Nature Communications **10** (2019) 3853.

[12] D. J. Hooton: Philos. Mag. **3** (1958) 49.

[13] Y. Oba, T. Tadano, R. Akashi, and S. Tsuneyuki: Physical Review Materials **3** (2019) 033601.

[14] T. Tadano, Y. Gohda, and S. Tsuneyuki: J. Phys: Condens. Matter **26** (2014) 225402.

[15] A. A. Maradudin and A. E. Fein: Phys. Rev. **128** (1962) 2589.

[16] T. Feng, L. Lindsay, and X. Ruan: Physical Review B **96** (2017) 72 .

[17] N. K. Ravichandran and D. Broido: Physical Review B **98** (2018) 1 .

[18] P. B. Allen and J. L. Feldman: Physical Review Letters **62** (1989) 645.

[19] P. B. Allen and J. L. Feldman: Physical Review B **48** (1993) 12581 .

[20] F. Zhou, W. Nielson, Y. Xia, and V. Ozoliņš: Phys. Rev. Lett. **113** (2014) 185501.

[21] T. Tadano and S. Tsuneyuki: Journal of the Physical Society of Japan **87** (2018) 041015 .

[22] M. Somayazulu, M. Ahart, A. K. Mishra, Z. M. Geballe, M. Baldini, Y. Meng, V. V. Struzhkin, and R. J. Hemley: Physical Review Letters **122** (2019) 027001.

[23] A. P. Drozdov, P. P. Kong, V. S. Minkov, S. P. Besedin, M. A. Kuzovnikov, S. Mozaffari, L. Balicas, F. F. Balakirev, D. E. Graf, V. B. Prakapenka, E. Greenberg, D. A. Knyazev, M. Tkacz, and M. I. Eremets: Nature **569** (2019) 528 .

[24] H. Liu, I. I. Naumov, R. Hoffmann, N. Ashcroft, and R. J. Hemley: Proceedings of the National Academy of Sciences **114** (2017) 6990.

[25] F. Peng, Y. Sun, C. J. Pickard, R. J. Needs, Q. Wu, and Y. Ma: Physical review letters **119** (2017) 107001.

[26] I. Errea, F. Belli, L. Monacelli, A. Sanna, T. Koretsune, T. Tadano, R. Bianco, M. Calandra, R. Arita, F. Mauri, and J. A. Flores-Livas: Nature **578** (2020) 66.

[27] T. Tadano and S. Tsuneyuki: Physical review letters **120** (2018) 105901.

[28] B. C. Sales, B. C. Chakoumakos, R. Jin, J. R. Thompson, and D. Mandrus: Phys. Rev. B **63** (2001) 245113.

[29] A. F. May, E. S. Toberer, A. Saramat, and G. J. Snyder: Phys. Rev. B **80** (2009) 125205.

[30] K. Suekuni, C.-H. Lee, H. I. Tanaka, E. Nishibori, A. Nakamura, H. Kasai, H. Mori, H. Usui, M. Ochi, T. Hasegawa, M. Nakamura, S. Ohira-Kawamura, T. Kikuchi, K. Kaneko, H. Nishiate, K. Hashikuni, Y. Kosaka, K. Kuroki, and T. Takabatake: Advanced Materials **285** (2018) 1706230 .

[31] T. Tadano, Y. Gohda, and S. Tsuneyuki: Phys. Rev. Lett. **114** (2015) 095501.

[32] T. Tadano. ALAMODE. https://github.com/ttadano/alamode.